



WHITEPAPER

# The GeoMx<sup>®</sup> Human Whole Transcriptome Atlas for the Digital Spatial Profiler:

## Design, Performance, and Experimental Guidelines

*Robin Fropf, Maddy Griswold, Stephanie Zimmerman, Karen Nguyen,  
Jason Reeves, Kit Fuhrman, Michael Rhodes*

FOR RESEARCH USE ONLY. Not for use in diagnostic procedures.  
NanoString Technologies, Inc., Seattle, WA 98109  
MK3209 | Sep 2022

nanoString<sup>®</sup>

## Summary

The GeoMx<sup>®</sup> Whole Transcriptome Atlas (WTA) uncovers the spatial heterogeneity of tissue sections using the GeoMx<sup>®</sup> Digital Spatial Profiler (DSP). In this report we've compared WTA to other technologies to bridge research from lower plex or bulk technologies and provide guidelines for WTA applications. This work utilizes the Human WTA but the guidance can be extended to other GeoMx RNA assays such as the Mouse WTA.

### Important Highlights

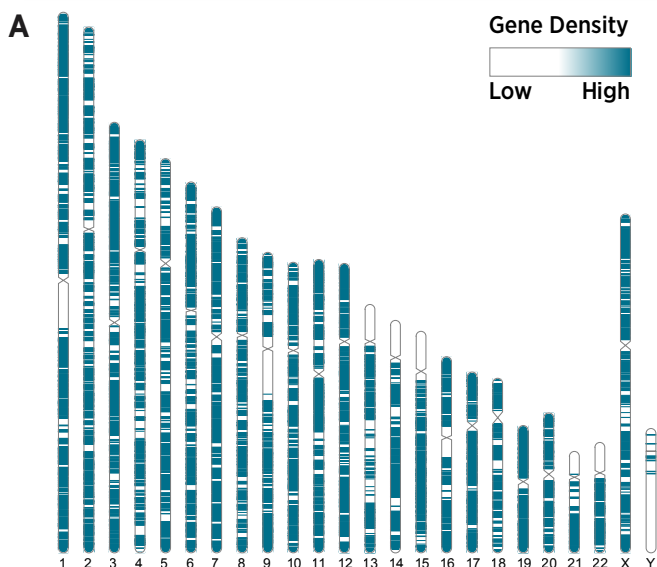
- WTA delivers high sensitivity and detects 6,000-12,000 genes per AOI in our tumor FFPE samples
- WTA detects low-expressing and high-expressing genes across a range of AOI sizes
- WTA is concordant with RNAseq and RNAscope
- Experimental recommendations for WTA use:
  - Plan for 100 reads/ $\mu\text{m}^2$  read depth to optimize WTA data quality for all analyses
  - AOIs with sequencing saturation lower than 50% should be filtered out of analysis
  - AOI size recommendations depend on experimental goals (see **Table 1**)

## Introduction

Translational and exploratory research require high-plex analyte profiling to examine cellular changes across biological systems. The recent launch of Digital Spatial Profiling with Next Generation Sequencing readout technology (DSP-NGS) enables a vast increase in the number of targets that can be profiled with DSP. Here, leveraging the DSP-NGS readout, we introduce the GeoMx Human Whole Transcriptome Atlas (WTA) for DSP and provide general guidelines for region selection to optimize performance.

WTA includes in situ hybridization probes designed to target 19,505 annotated RNA targets (some probes target multiple genes) and 99.5% of the protein-coding genes defined in the HUGO database (**Figure 1a**). Of the omitted genes in WTA, ten nuclear genes and thirteen mitochondrial genes with extremely high expression were intentionally removed to optimize readout efficiency (**Figure 1b**). Though mitochondrial transcript levels vary widely by tissue type (Mercer et al, 2011), the 23 genes removed in WTA can comprise up to 40% of polyadenylated transcripts in a cell. Creating a curated WTA by removing these 23 genes therefore provides a significant advantage over a poly-A transcriptome in the percent of a sequencing run dedicated to biologically informative genes. The WTA marks a significant milestone in DSP target plex given its 10-fold increase in targets over the existing Cancer Transcriptome Atlas (CTA).

To understand the performance of a high-plex, single-tile design, we undertook a series of experiments to benchmark WTA against bulk RNAseq, CTA, and RNAscope in cell lines.



**B**

Top ten Expressed		Mitochondrial	
PSAP	EEF1A1	MT-CO2	MT-ND1
UBC	ACTG1	MT-ATP6	MT-ND3
ACTB	EEF2	MT-ND2	MT-ND5
TPT1	FTL	MT-ND4L	MT-ND6
RPL3	GAPDH	MT-ND4	MT-CO1
		MT-CO3	MT-ATP8
			MT-CYB

**FIGURE 1: INTRODUCTION TO WTA. A.** Ideogram illustrating the density of genes WTA detects across the genome. **B.** Table showing the 23 genes removed from WTA content in order to optimize sequencing efficiency.

We also performed in silico subsampling on sequencing results from experiments done in tissue to determine the effect of read depth on analysis results. Together, our results demonstrate that WTA successfully facilitates transcriptome-scale spatial biology for discovery-focused research projects.

### WTA has High Sensitivity and Good Concordance with RNAseq

To benchmark WTA against bulk RNAseq, we first examined WTA performance in Formalin-Fixed Paraffin Embedded (FFPE) Cell Pellet Arrays (CPAs) with matched CTA data. We compared both WTA and CTA data to transcripts per million (TPM) counts from a publicly available bulk RNAseq dataset in the Cancer Cell Line Encyclopedia (CCLE, Ghandi et al 2019). Each CPA experiment involved differently sized circular Areas of Interest (AOIs) to test technical performance across a range of conditions.

We first compared signal between WTA and other assays, with scatterplots illustrating concordance in a representative cell line (**Figure 2a**). Each scatterplot compares WTA signal on the y axis and CTA or RNAseq on the x axis, grouped by AOI size in DSP. We observed a linear correlation between CTA and WTA, indicating similar performance between WTA and previously developed DSP readouts. WTA maintains good concordance with RNAseq for genes expressed above TPM of 1 in RNAseq. Across all cell lines, correlation coefficients increased as WTA AOI size increased, and were above 0.75 for all comparisons to WTA with circle AOIs 200µm or larger (**Figure 2b**).

We next investigated the sensitivity of the WTA readout by making binary expression calls (expressed or not) for each gene, in each AOI, across all the datasets. Using the RNAseq results as ground truth, we calculated whether each call in the DSP data was a true positive, true negative, false positive, or false negative. We found similar sensitivity and specificity between CTA and WTA (**Figure 3**). For example, in 200µm AOIs both

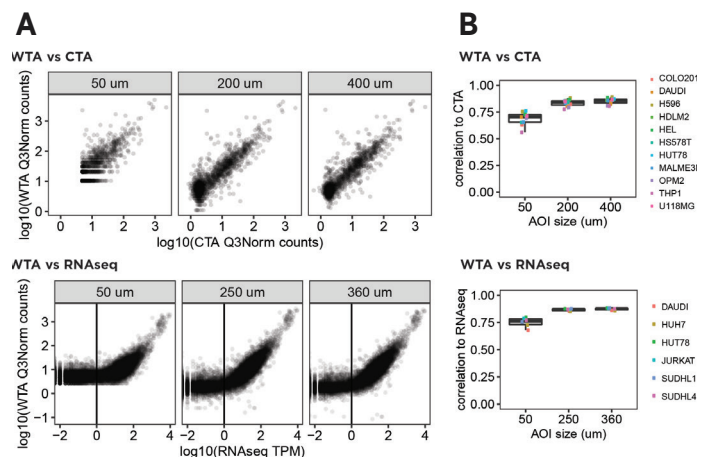


**FIGURE 2: WTA PERFORMANCE COMPARED TO CTA AND RNASEQ.** **A.** Scatterplots of normalized WTA counts compared to normalized CTA counts and bulk RNAseq TPM for a representative cell line. **B.** Spearman's correlations of normalized WTA counts to normalized CTA counts and bulk RNAseq TPM for all genes common to the pair of datasets being compared (dots indicate individual cell lines).

CTA and WTA detect about 70% of the genes predicted to be expressed based on RNAseq, despite the thousands of cells as input into standard bulk RNAseq protocols compared to the hundreds of cells that go into DSP datasets. Additionally, while we observed lower sensitivity in smaller, 50µm diameter AOIs, we found high specificity across all AOI sizes (**Figure 3b**).

Finally, we used the comparison between WTA and RNAseq to perform breakpoint analysis and determine at what TPM level we start detecting signal above noise with WTA. The breakpoint analysis fits two line segments to the data and iteratively calculates the breakpoint at which the model best fits the data. An example of a breakpoint calculation for one comparison is shown in **Figure 4a**, with the vertical red line indicating the calculated breakpoint and the two blue lines indicating the two fit lines on either side of the breakpoint. We calculated breakpoints across all cell lines and AOI sizes (**Figure 4b**). Breakpoints were around TPM of 2 in larger AOIs, but were much higher in smaller AOIs, illustrating the tradeoff between sensitivity and cell number.

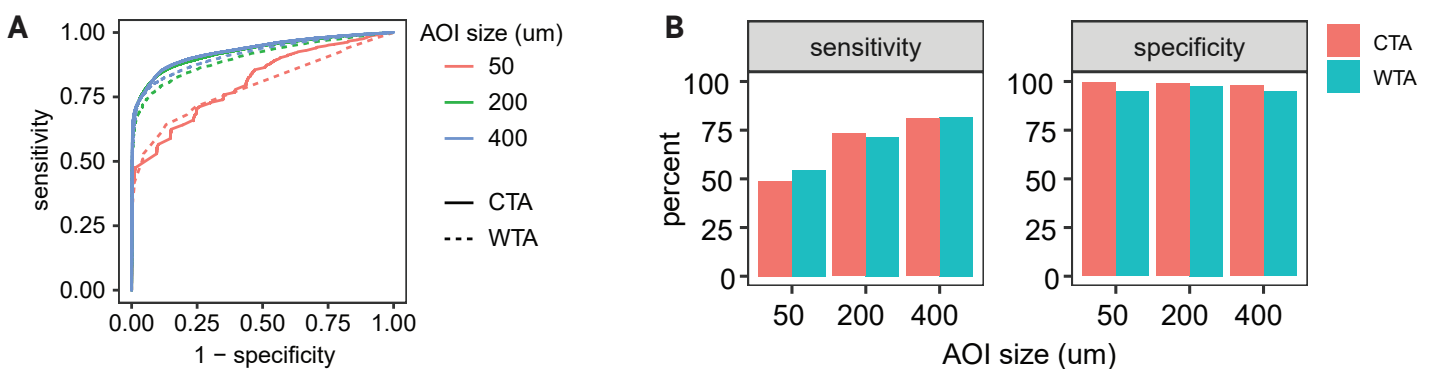


**FIGURE 3. WTA SENSITIVITY AND SPECIFICITY COMPARED TO CTA.** **A.** Using RNAseq TPM as truth for the expression call of each gene, we plotted a ROC curve to assess how well WTA and CTA can detect genes as expressed in different AOI sizes. **B.** Sensitivity and specificity numbers for each AOI size.

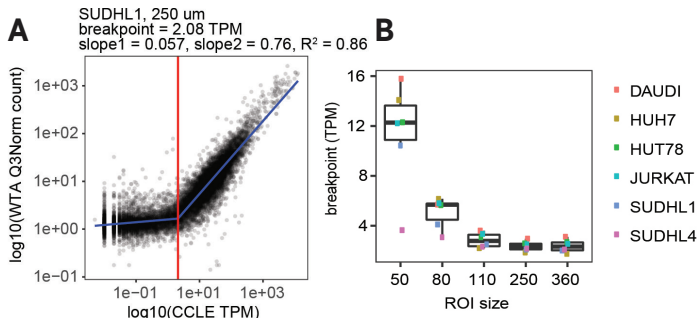


**FIGURE 4. BREAKPOINT ANALYSIS SHOWS WHERE WTA STARTS TO DETECT SIGNAL ABOVE NOISE. A.** Scatterplot showing results of breakpoint analysis for a representative cell line. Red line indicates calculated breakpoint. **B.** Calculated breakpoints across all cell lines and AOI sizes.

### Absolute Transcript Number Detection Capabilities of WTA

We next wanted to benchmark WTA performance against RNAscope, a technology capable of detecting single RNA molecules. We integrated WTA data with RNAscope experiments that counted number of transcripts present per cell for individual genes (**Figure 5a**). We then plotted normalized WTA counts as a function of the estimated number of transcripts per cell within that AOI. With this comparison, we performed breakpoint analysis at different AOI sizes and found that we can start detecting WTA signal at 0.5-2 transcripts per cell, depending on AOI size (**Figure 5b**, table of breakpoint values per AOI size on right).

Using the WTA/RNAscope comparison, we then calculated WTA sensitivity based on the number of cells in the AOI and the gene expression level of the target (**Figure 5c**). Highly-expressed transcripts (above 10 transcripts/cell) are detected in all AOI sizes while lower-expressed transcripts (below 10 transcripts/cell) have more graded performance, depending on AOI size (**Figure 5c**).

Given the results from our breakpoint analysis and our sensitivity calculations, we conclude that WTA detects high- and mid-expressing targets with a range of AOI sizes, but low expressed targets would benefit from larger AOI sizes for increased confidence.

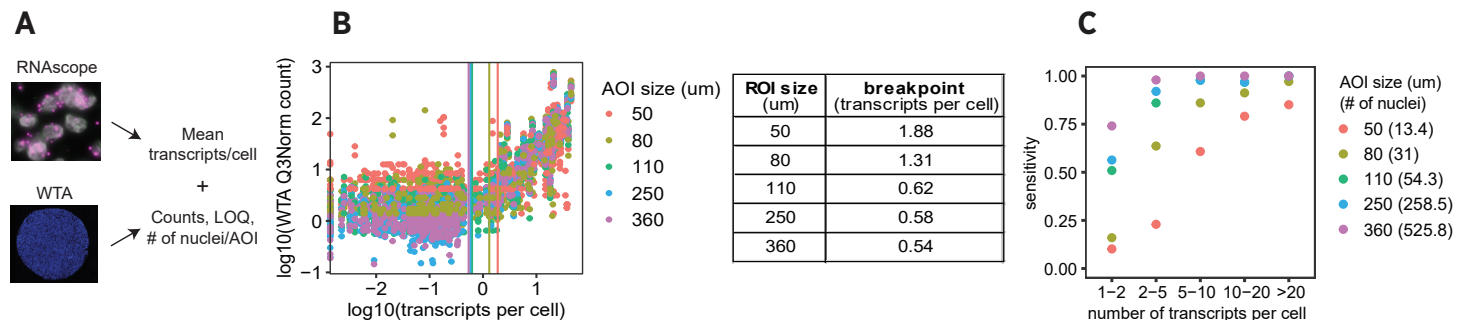


**FIGURE 5. ABSOLUTE LIMIT OF QUANTITATION OF WTA. A.** Schematic of the method for integrating RNAscope transcripts per cell with WTA counts and nuclei per AOI. **B.** Scatterplot of estimated transcripts per cell for each gene compared to normalized WTA counts. Points are colored by AOI size. Vertical lines indicate the breakpoint in for each AOI size. **C.** Sensitivity of WTA binned by estimated transcripts per cell from RNAscope. Points are colored by AOI size with the average number of nuclei at each AOI size listed.

We next looked further into how AOI size affects biological analyses. Using an experiment with a range of AOI sizes across two FFPE cancer tissues (see experiment explanation in **Figure 6**), we binned AOIs into different size ranges and calculated secondary analysis outputs for each bin. Next, we calculated Spearman's correlations between each AOI within a category (tumor or immune) and plotted the correlation coefficients based on the size of each AOI. We then averaged the results by AOI size bin to summarize trends and found that correlations decrease as AOI size decrease (**Figure 8**). Some of this decrease is almost certainly biologically driven by smaller AOI sizes having a more restricted sampling of the cellular populations in a heterogenous tissue. However, some of this decrease is likely a result of loss of technical performance in smaller AOI sizes, as matches the results seen in CPA experiments with more homogenous sample types (**Figures 2-5**).

In both cell and tissue experiments, we observed a gradual decrease in performance with no obvious threshold under which WTA fails to measure the biology of the sample. However, we did observe the biggest apparent drop in data quality in AOIs with areas less than 100µm diameter circle equivalents (around a hundred cells minimum), as measured by correlations to RNAseq in cell lines and correlations to larger AOI sizes in tissue.

### Subsampling Sequencing Data to Determine Ideal Sequencing Depth for WTA

We next examined unique morphological structures in colorectal cancer (CRC) and non-small cell lung cancer (NSCLC) to build out sequencing guidelines for WTA in FFPE tissue (**Figure 6a**). To profile the biology of these samples, we collected AOIs from different regions of the tissue (Tumor, Hyperproliferative, Invasive Margin defined by a pathologist) and segmented for immune content (+/- PanCK). Additionally, we titrated AOI size and calculated number of cells present per AOI to determine how cell input affects WTA results (**FIGURE 6C**). The libraries

prepared from these AOIs were over sequenced to a median reads/ $\mu\text{m}^2$  of 325, far higher than what we estimated would be necessary based on CTA recommendations. We then selected the 212 AOIs with a sequencing depth of at least 300 reads/ $\mu\text{m}^2$ , performed five replicates of in silico subsampling of fastq files using seqtk (<https://github.com/lh3/seqtk>). We confirmed the subsampling worked by plotting read depth vs unique molecular identifier (UMI) % unique, or the proportion of the library complexity that has been sequenced, and confirmed that increasing read depth reduces % unique (**FIGURE 6B**). The resulting size distribution of AOIs included in the analysis summarized in the table in **FIGURE 6D**.

We next looked at primary and secondary analysis in our subsampled dataset to probe the potential to detect meaningful biological differences at different sequencing depths.

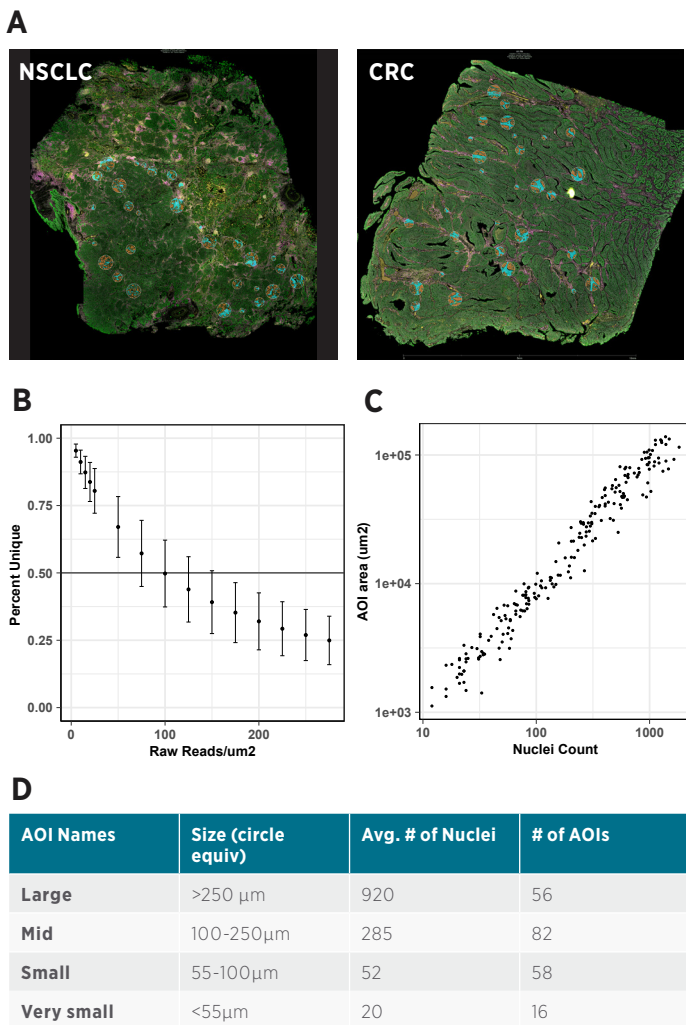


**FIGURE 6: SUBSAMPLING METHOD TO DETERMINE IDEAL READ DEPTH.** **A.** Colorectal cancer (CRC) and non-small cell lung cancer (NSCLC) tissues were used for the experiment. **B.** As read depth increases, UMI % unique goes down, confirming that subsampling worked. **C.** AOI size and nuclei count are directly proportional. **D.** Description of AOI size bins in terms of size of the equivalent circle of appropriate diameter as well as the number of AOIs in each size bin.

First, we assessed the correlation of normalized counts values for each sequencing depth to the deeply sequenced 300 reads/ $\mu\text{m}^2$  data (**Figure 7a**). Importantly, count correlation were well maintained for all but the low sequencing depths. We next found that the number of genes detected increases as sequencing depth increases, with median numbers of genes called as expressed plateauing by 100 reads/ $\mu\text{m}^2$  (**Figure 7b**). We also found increased numbers of genes detected at larger AOI sizes for all sequencing depths, corroborating CPA results (**Figures 3, 5**).

Next, each subsampled AOI was compared to a fully-sequenced AOI for three different types of secondary analysis: cell type deconvolution (SpatialDecon), single sample Gene Set Enrichment Analysis (ssGSEA), and Differential Expression (DE) Fold Change (FC) and p-value (Pval). The segmentation of tumor vs immune

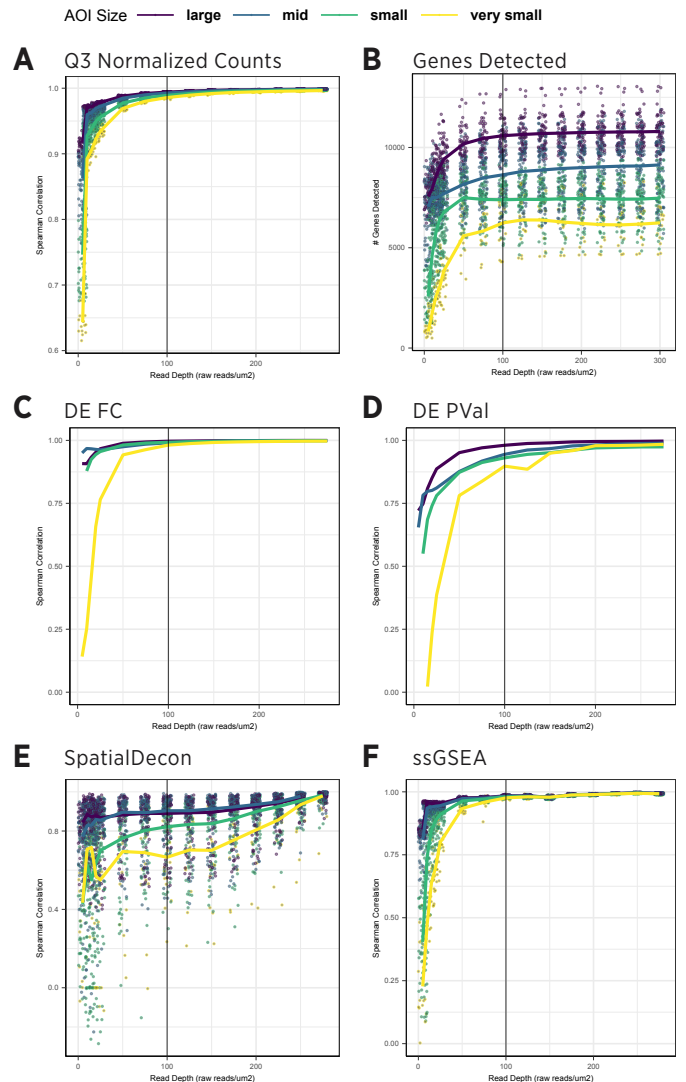


**FIGURE 7: SUBSAMPLING ANALYSIS TO IDENTIFY IDEAL READ DEPTH WITH HUWTA.** **A.** Correlation of subsampled Q3 normalized counts values (Q3) to more deeply sequenced values. **B.** Number of genes detected per AOI at different read depths, split out by AOI size bins. **C-E.** Summary of different secondary analysis metrics at different read depths correlated to the 300 reads/ $\mu\text{m}^2$  'truth' dataset for each AOI.

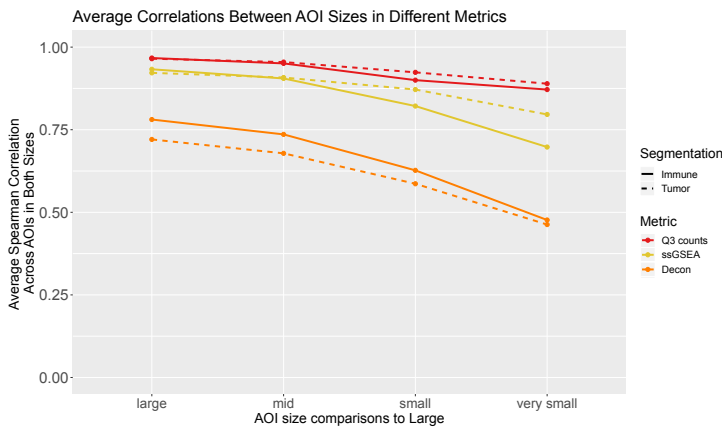


**FIGURE 8: SECONDARY ANALYSIS METRIC CORRELATIONS BETWEEN AOIS OF DIFFERENT SIZE BINS.** For three analysis output metrics (Cell decon, Q3 counts, ssGSEA), Spearman's correlations were calculated between each AOI, averaged within different AOI size bins compared to the largest AOI sizes. AOIs were split into groups based on AOI type (Immune and Tumor).

AOIs were used for the DE test. For each analysis, we calculated a Spearman's correlation coefficient of the subsample to the highest-sequenced dataset of the same AOI. As with genes detected, all AOI sizes showed poorer performance at low sequencing depths and performance on each metric peaked at a different read depth depending on AOI size (Figure 7c-e). Signal correlation, DE FC, ssGSEA are all relatively stable by 50 reads/ $\mu\text{m}^2$  for all AOI types; however, genes detected, DE Pval, and cell deconvolution metrics plateau by 100 reads/ $\mu\text{m}^2$  for large and medium AOIs and seem less stable at all read depths for small and extra small AOIs. We also looked at these metrics as a function of the fraction of the NGS library complexity that has been sequenced and found results to be robust above 50% sequencing saturation (data not shown).

Finally, to confirm that these sequencing depth recommendations are appropriate across diverse tissue types, we assessed sequencing saturation as a function of read depth across numerous tissue types (Figure 9). Each color indicates a different experiment, with individual points showing sequencing saturation per AOI within that experiment. This analysis of 19 experiments across tissue types shows that a read depth of 100 reads/ $\mu\text{m}^2$  is

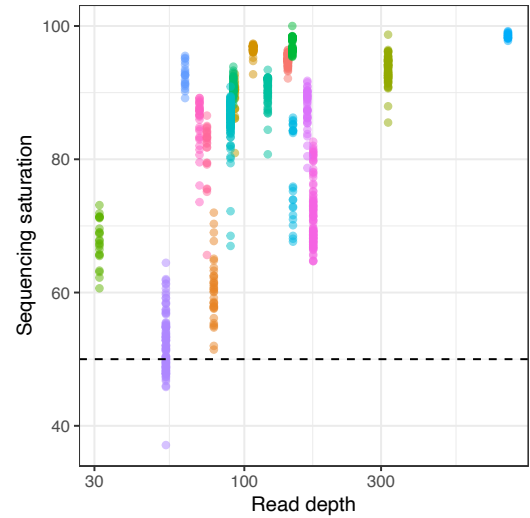


**FIGURE 9. SEQUENCING SATURATION AS A FUNCTION OF READ DEPTH ACROSS MULTIPLE TISSUES.**

consistently sufficient to get sequencing saturation above 50%.

We therefore recommend that users aim for WTA sequencing capacity of 100 reads per square micron when planning a sequencing run and use a QC cutoff of above 50% sequencing saturation when determining if individual AOIs were sequenced deeply enough.

### Conclusion

Given that specific desired analyses require different read depths and AOI sizes, we recommend each WTA user design their experiment with the results from Figures 1-8 taken into consideration. For example, detecting low-expressing genes will require more sequencing depth and larger AOIs than identifying differences in pathway analysis. However, anticipating that many researchers will request the smallest AOIs possible with WTA, based on these experiments we recommend a minimum read goal of 100 reads/ $\mu\text{m}^2$ , a sequencing saturation threshold of 50%, and a minimum AOI size of 100 $\mu\text{m}$  or 100 cells to optimize analytical outputs for WTA experiments. Future work will look at effects of different tissue types and quality on read depth requirements and AOI size guidelines.

	Small AOIs	Medium AOIs	Large AOIs
Area (circle diameter equivalent)	50 $\mu\text{m}$	100-200 $\mu\text{m}$	250 $\mu\text{m}$
Number of cells	15	100	250
Detect medium- and high-expressing genes	✓	✓	✓
Detect enriched pathways	✓	✓	✓
Robust cell type deconvolution		✓	✓
Robust differential expression analysis		✓	✓
Detect low expressing genes			✓

**TABLE 1:** List of analysis results detected by differently-sized features.

## References

- 1 Ghandi M, et al. Next-generation characterization of the Cancer Cell Line Encyclopedia. Nature. 2019 May;569(7757):503-508. doi:10.1038/s41586-019-1186-3. Epub 2019 May 8. PMID: 31068700; PMCID: PMC6697103.
- 2 Mercer TR, Neph S, Dinger ME, et al. The human mitochondrial transcriptome. Cell. 2011;146(4):645-658. doi:10.1016/j.cell.2011.06.051
- 3 Danaher P (2020). SpatialDecon: Deconvolution of mixed cells from spatial and/or bulk gene expression data. R package version 1.0.0.
- 4 Hänzelmann, S., Castelo, R. and Guinney, A. GSVA: gene set variation analysis for microarray and RNA-seq data. BMC Bioinformatics, 14:7, 2013.
- 5 Kuznetsova, A, Brockhoff, PB, Christensen RHB (2017). "lmerTest Package: Tests in Linear Mixed Effects Models." Journal of Statistical Software, \*82\*(13), 1-26. Doi: 10.18637/jss.v082.i13 (URL: <http://doi.org/10.18637/jss.v082.i13>).

For more information, please visit [nanosttring.com](https://nanosttring.com)

---

#### NanoString Technologies, Inc.

530 Fairview Avenue North  
Seattle, Washington 98109

T (888) 358-6266  
F (206) 378-6288

[nanosttring.com](https://nanosttring.com)  
[info@nanosttring.com](mailto:info@nanosttring.com)

#### Sales Contacts

United States [us.sales@nanosttring.com](mailto:us.sales@nanosttring.com)  
EMEA: [europe.sales@nanosttring.com](mailto:europe.sales@nanosttring.com)

Asia Pacific & Japan [apac.sales@nanosttring.com](mailto:apac.sales@nanosttring.com)  
Other Regions [info@nanosttring.com](mailto:info@nanosttring.com)

**FOR RESEARCH USE ONLY. Not for use in diagnostic procedures.**

© 2022 NanoString Technologies, Inc. All rights reserved. NanoString, NanoString Technologies, nCounter, nSolver, IO360, 3D Flow, Vantage 3D, and 3D Biology are registered trademarks of NanoString Technologies, Inc., in the United States and/or other countries.

SEP 2022 MK3209

**nanoString**  
